WiPhone: smartphone-based respiration monitoring using ambient reflected WiFi signals

Jinyi Liu, Youwei Zeng, Tao Gu, Leye Wang, Daqing Zhang

WiPhone: Smartphone-based Respiration Monitoring Using Ambient Reflected WiFi Signals

JINYI LIU, Peking University, China
YOUWEI ZENG, Peking University, China
TAO GU, Macquarie Univerisity, Australia
LEYE WANG, Peking University, China
DAQING ZHANG*, Peking University, China and Telecom SudParis, France

Recent years have witnessed a trend of monitoring human respiration using Channel State Information (CSI) retrieved from commodity WiFi devices. Existing approaches essentially leverage signal propagation in a Line-of-Sight (LoS) setting to achieve good performance. However, in real-life environments, LoS can be easily blocked by furniture, home appliances and walls. This paper presents a novel smartphone-based system named WiPhone, aiming to robustly monitor human respiration in NLoS settings. Since a smartphone is usually carried around by one subject, leveraging directly-reflected CSI signals in LoS becomes infeasible. WiPhone exploits ambient reflected CSI signals in a Non-Line-of-Sight (NLoS) setting to quantify the relationship between CSI signals reflected from the environment and a subject's chest displacement. In this way, WiPhone successfully turns ambient reflected signals which have been previously considered "destructive" into beneficial sensing capability. CSI signals obtained from smartphone are usually very noisy and may scatter over different sub-carriers. We propose a density-based preprocessing method to extract useful CSI amplitude patterns for effective respiration monitoring. We conduct extensive experiments with 8 subjects in a real home environment. WiPhone achieves a respiration rate error of 0.31 bpm (breaths per minute) on average in a range of NLoS settings.

CCS Concepts: • **Computer systems organization** → **Embedded systems**; *Redundancy*; Robotics; • **Networks** → Network reliability.

Additional Key Words and Phrases: Respiration Monitoring, WiFi, Smartphone, Channel state information, Ambient Reflection Signal Model

ACM Reference Format:
Jinyi Liu, Youwei Zeng, Tao Gu, Leye Wang, and Daqing Zhang. 2021. WiPhone: Smartphone-based Respiration Monitoring Using Ambient Reflected WiFi Signals. *Proc. ACM Interact. Mob. Wearable Ubiquitous Technol.* 5, 1, Article 23 (March 2021), 19 pages. https://doi.org/10.1145/3448092

*This is the corresponding author

Authors' addresses: Jinyi Liu, Peking University, Key Laboratory of High Confidence Software Technologies (Ministry of Education), School of Electronics Engineering and Computer Science, Beijing, China, liujinyi@pku.edu.cn; Youwei Zeng, Peking University, Key Laboratory of High Confidence Software Technologies (Ministry of Education), School of Electronics Engineering and Computer Science, Beijing, China, ywzeng@pku.edu.cn; Tao Gu, Macquarie Univerisity, Department of Computing, Macquarie University, Sydney, Australia, tao.gu@mq.edu.au; Leye Wang, Peking University, Key Laboratory of High Confidence Software Technologies (Ministry of Education), School of Electronics Engineering and Computer Science, Beijing, China, leyewang@pku.edu.cn; Daqing Zhang, Key Laboratory of High Confidence Software Technologies (Ministry of Education), School of Electronics Engineering and Computer Science, Peking University, Beijing, China , IP Paris, Telecom SudParis, Evry, France, dqzhang@sei.pku.edu.cn.

2474-9567/2021/3-ART23 $15.00
https://doi.org/10.1145/3448092

1 INTRODUCTION

Monitoring human respiration plays a vital role in people's daily health. A recent report from the International Respiratory Societies shows that chronic obstructive pulmonary disease and asthma affect more than 500 million people worldwide [11]. The high incidence of respiration diseases demands for effective, long-term and low-cost respiration monitoring, especially in home settings. Among the metrics of monitoring human respiration, respiratory rate has been widely used to track respiration diseases and predict paroxysmal disease as cardiac arrest [1].

Respiration monitoring is traditionally done in a clinical setting where patients are required to wear devices such as pulse oximeter [31] and capnometer [25] for continuous monitoring. However, these devices are proprietary and usually expensive. Commercial devices including pressure sensor [39] and activity sensor [27] have also been used. However, wearable devices may be intrusive, hence they are impractical for daily use in home settings. In contrast, a contactless approach is more attractive, as it has the distinct advantage of not requiring the attachment of electrodes to the subject's body. For instance, Doppler radar [8], FMCW radar [3] and UWB radar [34] have been used to detect human respiration in a contactless manner. Although they can achieve a relatively high accuracy, they are proprietary and costly (i.e., usually hundred dollar range). In recent years, WiFi signals have been explored for respiration monitoring [12, 20–22, 35, 37, 38, 40, 43–46, 48] due to the wider availability and low cost of WiFi infrastructure.

Existing WiFi-based respiration monitor systems usually require a subject presented on or close to the LoS between a pair of WiFi transceivers, as shown in Fig. 1. The systems exploit LoS signal paths reflected directly from human chest, i.e., signal paths are not blocked, and then apply signal propagation models to associate WiFi signal variations with chest movement. They work well in LoS scenarios where WiFi transceiver is placed at fix position with clear LoS (e.g., mounted on the ceiling above the bed or placed in front of the couch in the living room). However, in real-world environments, the directly-reflected paths via human chest may not always exist because they can be easily blocked by furniture, walls, and household appliances in a home setting, thus greatly limiting their practical applications. Few works investigate the Non-line-of-Sight (NLoS) scenarios for human respiration monitoring.

With the popularity of WiFi-based respiration monitoring, in this paper, we use off-the-shelf smartphone and commodity WiFi router as a pair of transceivers, aiming to provide robust respiration monitoring in NLoS settings. Existing systems use a mini-PC/laptop equipped with an Intel 5300 WiFi card to extract CSI signals. However, this card supports IEEE 802.11n only with a maximum bandwidth of 20 MHz. Today's smartphones support both 802.11n and 802.11ac, offering a maximum bandwidth of 80 MHz. Encouraged by the recent development of smartphone CSI tool Nexmon [29][30], we can retrieve CSI signals from about 10 different off-the-shelf smartphones. Different from the data injection model adopted in the existing systems based on Intel 5300 card, we extract CSI signals from WiFi beacon broadcast frames instead of data frames. In this way, respiration monitoring can be done passively, where no additional WiFi traffics are generated and no extra bandwidth is consumed at router. Due to its better mobility compared to mini-PC or laptop, smartphone is usually carried by a subject on a day-to-day basis. This makes smartphone an ideal receiving device for wireless human respiration monitoring in home settings, especially for people living alone and using smartphone often at home. However, designing an effective respiration monitoring system based on smartphone faces several technical challenges.

First, CSI signals extracted from smartphone present a relatively poor quality compared to that from Intel 5300 WiFi card. The state-of-the-art, FarSense [45], proposes the ratio of CSI readings from two antennas to cancel out most of the noise in both CSI amplitude and phase. However, this method does not work for smartphone which typically has only one single antenna. Besides, we observe that the raw CSI signal obtained by smartphone is very noisy, may not be able to use directly for respiration sensing. Second, in a typical home setting, it is difficult to guarantee the directly-reflected signal path via human chest since a WiFi router is usually placed at a fixed

location (e.g., a corner) and a smartphone is carried around by a subject. In many cases, such path may be blocked by the subject. Fig. 2 illustrates a NLoS scenario where both LoS and directly-reflected signal paths are blocked by obstacles, i.e., wall or furniture.

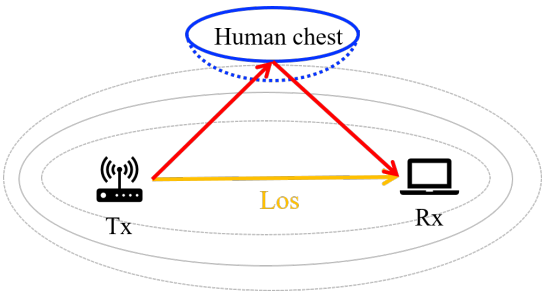

Fig. 1. Respiration monitoring in the LoS scenario

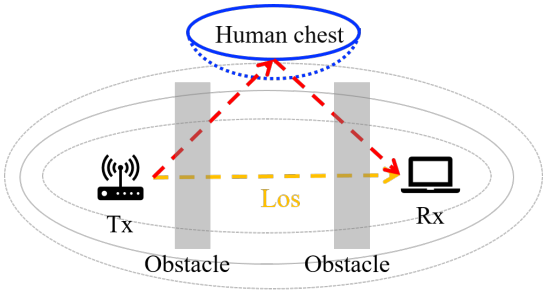

Fig. 2. Respiration monitoring in the NLoS scenario

To address the aforementioned challenges, we first study the feasibility of ambient reflected signal paths in the NLoS setting for respiration monitoring. Multiple paths reflected from the environment are usually ignored in previous works and even considered as harmful noise. In this paper, we turn the "destructive" reflection signals into constructive sensing capability and analyze CSI signal variations caused by human breathing. For the first time, we propose an ambient reflection signal model under the NLoS setting to obtain CSI amplitude variations at receiver which vary with the fine-grained displacement of human chest. We apply DBSCAN, a density-based clustering algorithm to cluster and select CSI samples which can be used to potentially represent respiratory patterns. We also propose a threshold selection method to select the best CSI samples from each sub-carrier for respiration sensing. The main contributions of the paper can be summarized as follows.

- We present a smartphone-based respiration monitoring system and propose an ambient-reflected signal model in the NLoS setting. This model greatly complements to the existing directly-reflected signal model that works only in LoS scenarios. We believe that this model offers a new possibility of applying ambient-reflected signal model to robust detection of human respiration in realistic settings.
- We exploit a DBSCAN-based clustering method to elaborately extract respiratory patterns from noisy CSI signals obtained from smartphone, and propose a threshold selection method to select the best CSI amplitude samples for each of the sub-carriers.
- We conduct extensive experiments with different NLoS scenarios in a real home environment, e.g., smartphone and WiFi router are placed in the same room, in different rooms with wall(s) in between, and etc. The results show that WiPhone achieves a respiration rate error of 0.31 bpm on average in various NLoS scenarios, outperforming the state-of-the-arts FarSense [45].

The rest of this paper is organized as follows. Section 2 surveys the related work. Section 3 describe the CSI signal preprocessing. Section 4 presents the ambient reflection model and applies this model to CSI signals. Section 5 presents the experiments and reports the results, and finally Section 6 concludes the paper.

2 RELATED WORK

This section discusses the most relevant works in respiration sensing with RF signals which can be divided in two categories: Radar-based and WiFi based.

Radar-based respiration sensing. The radar-based approaches rely on the modulation effect (due to chest displacement) of radio signals sent by a transceiver towards a subject. Three types of radar are commonly used

in the literature–Continuous-Wave (CW) Doppler radar, Ultra-Wideband (UWB) pulse radar and Frequency-Modulated Continuous-Wave (FMCW) radar.

(1) CW Doppler radar emits a radio signal with constant frequency and amplitude, detecting respiration by the received signal which is reflected off a moving chest [7, 9]. Compared with other types of radar, CW radar has a relatively simple architecture and low power consumption. However, CW radar signals may be easily affected by environmental noise.
(2) UWB pulse radar emits ultra-short pulses to a subject and receives the echo signals in the silent period [33]. The received signal can be visualized in frequency domain, the accurate estimation in time domain is extracted by Inverse Fast Fourier Transform (IFFT) [14, 18]. Compared with CW radar, the 1-2 GHz bandwidth makes UWB pulse radar able to eliminate interference caused by reflection from other objects and multipath [19]. A wide bandwidth improves the performance of sensing, but inevitably increases the hardware cost and complexity [17].
(3) FMCW radar emits continuous wave signals like CW radar but a signal is modulated with a liner increasing frequency in a wide channel band (1-2 GHz) [32]. FMCW radar is originally used to accurately measure the distance between transceiver and target. Vital-Radio [3] uses FMCW radar to separate signals from different subjects based on the signal's propagation time and using FFT to separate their respiration rate and heart rate. DeepBreath [42] recovers the respiration signals of multiple individuals from FMCW signals using Independent Component Analysis [4]. Compared with commodity Wi-Fi devices, FMCW radar uses a much wider bandwidth (1.5 GHz) in [42].

WiFi-based respiration sensing. The WiFi-based approaches can be divided into two categories as follows.

(1) Pattern-based respiration sensing. Abdelnasser *et al.* [2] make the first attempt to monitor human respiration leveraging the change of WiFi Received Signal Strength (RSS) patterns that correspond to the breathing process. However, RSS is insensitive to the minute chest displacement movements during respiration and can thus be easily overwhelmed by the noise [23]. The drawback prevents it from detecting respiration reliably in natural settings. Compared with RSS, CSI is more sensitive to chest displacement. Wi-Sleep [21] presents the first sleep monitoring system which extracts signal patterns caused by chest displacement from WiFi CSI. The authors further improve the performance in [22] and consider sleeping postures and abnormal respiration patterns at the same time. TensorBeat [38] and PhaseBeat [37] exploit CSI phase difference between two receivers' antennas to extract respiration rate. These systems are mainly based on the periodicity of signal patterns, but they are unaware of why RSS or CSI could be utilized for respiration sensing.
(2) Model-based respiration sensing. The **Fresnel Zone model** is first introduced in [35, 41, 47] for WiFi sensing. Wang *et al.* [35] apply this model to human respiration and reveal that the performance is subjected to user location (i.e., "blind spots"). FullBreathe [43] demonstrates the complementarity between CSI phase and amplitude for respiration sensing and proposes to employ both amplitude and phase to remove "blind spots". A recent work [48] further consider the diffraction effects during respiration inside the first Fresnel zone and qualify the relationship between the diffraction gain and the target location for respiration sensing. These systems leverage the directly-reflected signal path via chest-wall for sensing, hence they require a subject located near the LoS. This implies that respiration sensing can only be done in a restricted area between a WiFi transceiver pair. FarSense [45] proposes a new metric called CSI ratio to cancel out most of the noise in CSI amplitude and phase, and it further develops the **CSI-ratio model** that establishes the relationship between human's movement and CSI ratio changes which lays the foundation to guide fine-grained sensing. Leveraging the multiple views provided by many CSI ratios, MultiSense [44] manages to simultaneously monitor the respiration of multiple persons. However, to calculate the CSI ratio, at least

two antennas are required at the receiver. Thus, it does not work for off-the-shelf smartphone that has only one available antenna.

Other contactless solutions detect sleep apnea events on smartphones by transforming the phone into an active sonar system that emits frequency-modulated sound signals and uses their reflections[26]. the state-of-the-art respiration systems [45][44] the authors only show NLoS experiments where two WiFi receivers are placed at the same height in two rooms separated by a wall, they didn't show whether human respiration can be extracted in other NLoS cases, e.g., through two walls and the transceivers are placed at different heights. Different from existing work, we exploit ambient reflection WiFi signals for respiration sensing in a NLoS setting. The proposed ambient reflection signal model quantifies the relationship between chest displacement caused by respiration and path length change of ambient reflected signal. WiPhone overcomes the limitation of the existing work in the scenarios where the LoS is blocked. In addition, it operates without interrupting normal WiFi communication traffic.

3 PREPROCESSING CSI SIGNALS

In this section, we first present the process of obtaining raw CSI signals from an off-the-shelf smartphone using Nexmon and show the complexity of extracting useful signal patterns compared to that obtained from a mini-PC equipped with an Intel 5300 WiFi card. We then propose a DBSCAN-based clustering method to preprocess noisy CSI signals and present our method that uses noisy and scattering raw CSI signals from smartphone for respiration sensing.

3.1 Raw CSI Signals from Smartphone

We first conduct our experiments to present raw CSI signals obtained from smartphone and mini-PC with an Intel 5300 WiFi card, respectively.

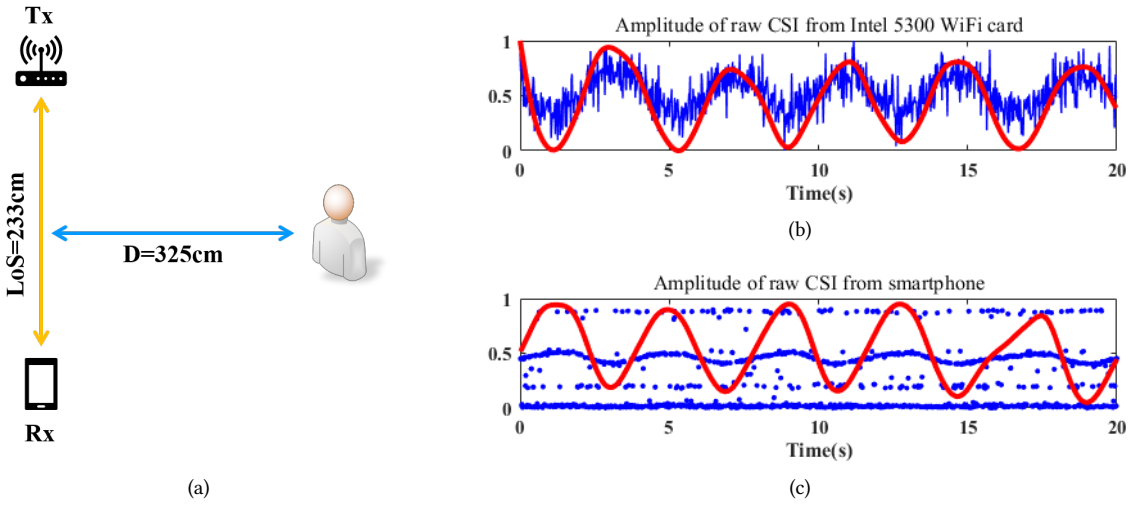

Fig. 3. Experiment setup in a LoS scenario (a), ground truth and CSI amplitude obtain from 5300 (b) and smartphone (c)

Experimental Setup We use a typical LoS scenario in existing WiFi-based respiration monitoring systems, as shown in Fig. 3 (a). A subject is located between a WiFi transceiver pair with the same height of 1.25 m and the

LoS length of 2.3 m. The subject breathes naturally and a commercial device (Neulog Respiration Monitor Belt Logger sensor NUL-236[16]) is used to collect the ground truth. We first use a mini-PC equipped with an Intel 5300 WiFi card as receiver to collect CSI signals, we then repeat the experiment by replacing the mini-PC with a Google Nexus 5 smartphone. In both experiments, the WiFi router works in 5 GHz band and the sampling rate is set to 50 Hz. We collect both CSI signals for a period of 20 seconds.

Fig. 3 (b) and (c) show the ground truth of respiration and the CSI amplitude obtained from mini-PC and smartphone, respectively, the ground truth is illustrated in red line and raw CSI amplitude is illustrated in blue line. We observe a clear sine wave that matches the ground truth of subject's respiration in Fig. 3 (b). However, in Fig. 3 (c) we observe that the CSI readings obtained by smartphone are noisy and scattered across multiple values. Furthermore, the CSI readings obtained from different smartphones present similar scattering characteristics when different commercial WiFi routers are used. Actually, the scattering is caused by the internal CSI estimation algorithm and automatic gain control (AGC) algorithm of the smartphone's WiFi NIC.

In this paper, we adopt DBSCAN in order to separate the respiration modulated CSI signal from the scattering and noises in the received CSI waveforms.

3.2 CSI Preprocessing

3.2.1 DBSCAN-based Clustering. We apply DBSCAN, a density-based clustering algorithm which does not require the predetermination of the number of clusters, it has the ability in discovering clusters with discretionary shape including but not limited to liner, curve and ring. This makes DBSCAN really suitable to cluster raw CSI amplitudes received from smartphone because the scattering characteristic for each sub-carrier is not the same, and unable to know beforehand. DBSCAN has been widely used in the fields of chemistry [6], spectroscopy [49], social sciences [10, 15] and medical diagnostics [5, 28]. There are two important parameters need to be pre-defined in DBSCAN:

- Eps: the maximum radius of the neighborhood from point p
- MinPts: the minimum number of points required to form a dense region

DBSCAN starts with an unlabeled point p in database D, and screens all the neighbors of p within a distance of Eps. If the number of neighbors is no less than $MinPts$, a new temporary cluster is created, point p and its neighbors will be classified into this temporary cluster. DBSCAN then walks through all the neighbors within the distance of Eps from p, classify the core object and its neighbors into the same cluster until no density-reachable point left. This process is repeated until all of the points have been processed, it groups the points that are closely packed together (i.e., points with many nearby neighbors). To measure the distance between a neighbor point and the core object, we use Euclidean distance $dist(i, j)$ which is defined as follows:

$$dist(i, j) = \sqrt{(i_x - j_x)^2 + (i_y - j_y)^2} \tag{1}$$

where $i = (i_x, i_y)$ and $j = (j_x, j_y)$ are two points in database , x presents the CSI amplitude of each package, y presents the timestamp of the package. However, the use of Euclidean distance may run into the problem when the distribution of each classes is uneven in time domain, a consecutive respiration pattern is clustered into different classes due to uneven distribution. As the scattering characteristic is time-independent, we add another distance based on amplitude difference as follows.

$$dist(i, j) = Amp_i - Amp_j \tag{2}$$

where Amp_i and Amp_j represents the amplitude of i and j, respectively. This implies that we directly use amplitude difference instead of Euclidean distance to present the distance between two points.

3.2.2 Pre-defined Parameters. DBSCAN requires two pre-defined parameters–$MinPts$ and Eps, representing the density of each cluster. Since each sub-carrier may have different CSI amplitude values, it is difficult, if not impossible, to find these optimal parameters to cluster all samples for all the sub-carriers. To maximize CSI signal patterns for each of the sub-carriers, we propose a self-adaptation algorithm to select the optimal parameter pair.

As the distance between two data points from the same cluster is closer than that from different clusters, we can use in-class and between-class distances to pre-define $MinPts$ and Eps. To be specific, we select CSI amplitudes in a certain period of time at the beginning of breathing. For each CSI sample, we first calculate the distance to other points using Eq.2, and then sort the distance in an ascending order, expressed as follows:

$$S_i = dis_{i,1}, dis_{i,2}, \cdots, dis_{i,j}, \cdots, dis_{i,N} \tag{3}$$

where n is the number of CSI samples in the period of time, $dis_{i,j}$ represents the jth smallest distance to the ith CSI sample. We calculate the mean value of all distance sequence S_i as follows:

$$S\_mean = \frac{1}{N}\sum_{i=1}^{N} dis_{i,1}, \frac{1}{N}\sum_{i=1}^{N} dis_{i,2}, \cdots, \frac{1}{N}\sum_{i=1}^{N} dis_{i,j}, \cdots, \frac{1}{N}\sum_{i=1}^{N} dis_{i,N} \tag{4}$$

The final sequence represents in-class and between-class distances during the time period. Here we select the value of the first "inflection point" (x, y) as $MinPts$ and Eps, i.e., $Eps = x/2$ and $MinPts = y$.

3.2.3 Best Candidate Selection. After clustering raw CSI amplitudes for each of the sub-carriers, from these candidates we now select the best cluster which represents respiration pattern. Based on the fact that the human respiration rate remains constant over a short period of time [42, 45], we leverage the periodicity of signals to select the best candidate. The periodicity of clusters in each sub-carrier can be measured using Breathing-to-Noise Ratio (BNR) [42] which is defined as a ratio of respiration energy to the overall energy. To compute BNR, the window length is set to 10s which contains 500 samples for all clusters. We first increase the number of samples from each cluster to 500 by linear interpolation. We then apply Fast Fourier Transform (FFT) and find the FFT bin with the maximal energy within the human respiration range (5 bpm to 37 bpm [45]). BNR can be then calculated by dividing the bin's energy by the energy sum of all FFT bins within the human respiration range as follows:

$$BNR_i = \frac{Maximal\_energy}{Total\_energy} \tag{5}$$

where BNR_i is the BNR value of candidate i classified by DBSCAN in a sub-carrier. For all the sub-carriers, if the maximal BNR value among all the candidates is larger than a pre-defined threshold, we select it to represent the respiration waveform for this sub-carrier, otherwise, we conclude that this sub-carrier does not contain any useful patterns for respiration sensing.

3.2.4 Clustering Result. We now apply our clustering algorithm to CSI signals collected from smartphone, we randomly select three out of all sub-carriers as shown in Fig. 4 (a-c). The clustering result is presented in Fig. 4 (d-f), and we observe that the CSI amplitudes in each of the sub-carriers are scattered across multiple values and the resulting CSI samples represent a clear respiration pattern from different sub-carriers, which will be used for respiration detection in the next section.

3.3 Respiration Rate Estimation

In this subsection, we estimate respiration rate by combining CSI amplitude samples from multiple sub-carriers as FarSense [45] did. We first calculate the auto-correlation of sub-carrier i which contains useful respiratory

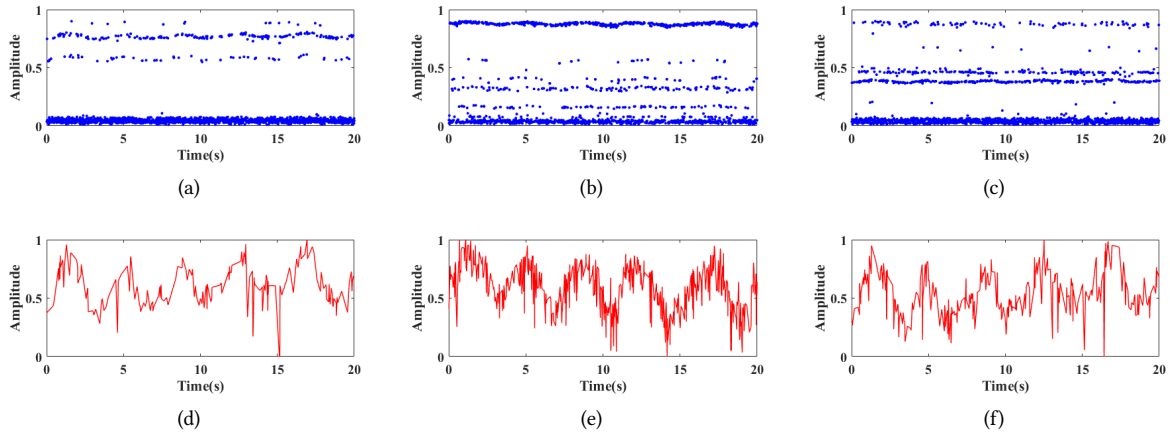

Fig. 4. Raw CSI amplitude (upper row) and CSI signal patterns obtained from preprocessing (lower row)

patterns. The auto correlation function describes the similarity of a signal to a shifted version of itself, defined as:

$$r_i(k) = \frac{\sum_{t=k+1}^{T} (y_i(t) - \overline{y_i}(y_i(t-k)) - \overline{y_i}}{\sum_{t=k+1}^{T} ((y_i(t) - \overline{y_i})^2} \tag{6}$$

where $r_i(k)$ is the auto-correlation for BNR_{comb} at a shift of k samples, y_i represents respiration pattern, T is the length of y_i, $\overline{y_i}$ is the mean of y_i, and k is number of samples shifted from 0 to $T-1$. We then combine each sub-carrier as:

$$r_{msc} = \sum (BNR_i) \times r_i(k) \tag{7}$$

The first peak of $r_{msc}(k)(k = 0, ..., T-1)$ is the component describing the periodicity of respiration. Finally, the shift of the first peak divided by the sampling rate presents the estimated period for one respiration cycle [45].

In summary, the CSI preprocessing method we presented in this section makes it possible to employ noisy CSI signals from smartphone for respiration sensing. It is worth noting that the proposed method can be applied to other WiFi-based applications such as indoor tracking and motion detection where smartphone is used as receiver. It can be also applied to other types of WiFi card and other wireless technologies which may be suffered from scattering. In this paper, we focus on applying this method to sensing human respiration in NLoS scenarios, and will present the detail in the following sections.

4 AMBIENT REFLECTION SIGNAL MODEL

This section first presents our ambient reflection signal model. We then apply this model to WiFi CSI signals and establish the corresponding relationship between CSI amplitude and chest displacement caused by respiration. We also analyze the two properties of this reflection model and verify them through experiments.

4.1 Modeling Respiration in Ambient Reflection Signals

Respiration sensing using smartphone can be tricky as smartphone is usually carried around by user. In many scenarios, the LoS between WiFi router and smartphone may be blocked by human body, wall and furniture in a

home environment. In this case, the directly-reflected signal path used in existing work does not exist. WiFi signals transmitted from the WiFi router may reflect via ambient environment (e.g., ceiling, wall and floor) multiple times before arriving at the smartphone, as illustrated in Fig. 5. In reality, the propagation of ambient-reflected signals can be very complex, but our intuition is that chest displacement may cause WiFi signal variations at receiver which can be exploited for respiration sensing.

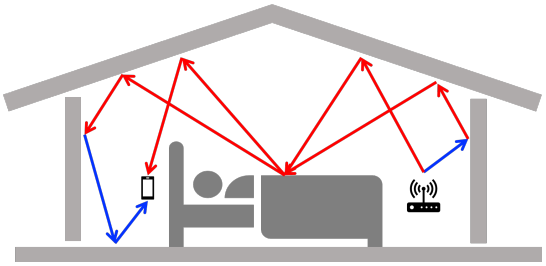

Fig. 5. Ambient reflection scenarios

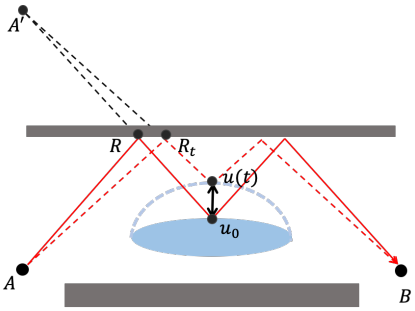

Fig. 6. Ambient reflection model with two reflection points

To simplify our analysis, we first use a scenario where the signal path has two ambient-reflected points, as shown in Fig. 6. The red dotted lines and solid lines illustrate the signal paths when a subject breaths in and out. A and B represents receiver and transmitter, respectively. u_0 represents the lowest chest point when breathing out. $d_i(t)$ and d_{i0} represents the total path length when breathing in and out, respectively. We focus our analysis on the left side from the human chest, and model the signal path length during breathing as follows:

$$d_i(t) = d_{i0} + \Delta d(t) = d_{i0} + k_i u(t) \tag{8}$$

where $\Delta d(t)$ denotes the length difference of two paths, $u(t)$ represents the chest displacement caused by respiration, k_i is a coefficient which may be different for each path. This coefficient defines the relationship between the path length change and the chest displacement. R_t represents the reflection point path change during breathing. Thus, the path change between A and the chest is:

$$\Delta d_A(t) = length(A - R_t - u(t)) - length(A - R_t - u_0) \tag{9}$$

As shown in Fig. 6, we extend u_0R and $R_tu(t)$ along their path, respectively, and the two paths intersect at $A^{'}$. Following the reflection law, it is easy to see that $\triangle ARR_t$ and $\triangle A^{'}RR_t$ are two congruent equilateral triangles, that is to say:

$$\Delta d_A(t) = length(ARC) - length(AR_tu(t)) = length(A^{'}Ru_0) - length(A^{'}R_tu(t)) \tag{10}$$

Obviously, the range of $\Delta d_A(t)$ is from 0 to $u(t)$. While the aforementioned analysis focuses on the left side of the chest, the right side follows the same principle. We hence generalize our model for multiple ambient-reflected points as follows:

$$d_i(t) = d_{i0} + k_i u(t) \ (0 < k_i < 2) \tag{11}$$

Note that the value range of K_i implies that the ambient-reflected path length change caused by respiration should be less than twice of chest displacement. In reality, the propagation of ambient-reflected signals in indoor environments can be very complex. Other scenarios which have more or less ambient-reflected points will be analyzed in Appendix 6.

4.2 Applying Ambient Reflection Model to WiFi CSI

WiFi CSI characterizes multipath propagation, and it is a superposition of signals from all the paths. Mathematically, CSI can be represented as follows:

$$H(f,t) = \sum_{i=1}^{L} A_i e^{-j2\pi \frac{d_i(t)}{\lambda}} \tag{12}$$

where L is the number of paths, A_i is the complex attenuation and $d_i(t)$ is the propagation length of the i th path. According to prior work [36], the paths can be classified into static path and dynamic path. Thus, the corresponding CSI can be written as:

$$H(f,t) = H_s(f,t) + H_d(f,t) = H_s(f,t) + \sum_{i=1}^{L} A_i(f,t) e^{-j2\pi \frac{d_i(t)}{\lambda}} \tag{13}$$

where $H_s(f,t)$ is the static component, $A(f,t)$, $e^{-j2\pi \frac{d_i(t)}{\lambda}}$ and $d(t)$ are the complex attenuation, phase shift and path length of dynamic component $H_d(f,t)$, respectively. As the change of $d_i(t)$ is caused by chest displacement as shown in Eq. 11, without loss of generality, we assume k_i for each ith path is of the arithmetic progression, which can be written as $k_i = k_0 + d(i-1)$, where k_0 is the beginning value and d represents the difference between two consecutive terms of the arithmetic progression. The CSI can be then written as:

$$H(f,t) = H_s(f,t) + \sum_{i=1}^{L} A_i(f,t) e^{-j2\pi \frac{d_{i0}+(k_0+d(i-1))u(t)}{\lambda}} \tag{14}$$

When the chest moves a short distance, the amplitude of the dynamic component $A_i(f,t)$ can be considered as a constant. This is because the amplitude is determined by the path length. The change of a few centimeters in path length has very little effect on this dynamic component. As $k_i = k_0 + d(i-1)$ is an arithmetic progression, according to the summation formulas of geometric progression, we can calculate that:

$$\sum_{i=1}^{L} e^{-j2\pi \frac{d_{i0}+(k_0+d(i-1))u(t)}{\lambda}} = \frac{sin(\frac{\pi}{\lambda} L du(t))}{sin(\frac{\pi}{\lambda} du(t))} e^{-j\frac{2\pi}{\lambda}(k_0+\frac{1}{2}dL)u(t)} \tag{15}$$

Thus, the received CSI from multiple paths presented in Eq. 14 can be rewritten as:

$$H(f,t) = H_s(f,t) + H_d(f,t) = H_s(f,t) + A(f,t)\frac{sin(\frac{\pi}{\lambda} dLu(t))}{sin(\frac{\pi}{\lambda} du(t))} e^{-j\frac{2\pi}{\lambda}(k_0+\frac{1}{2}dL)\cdot u(t)} \tag{16}$$

Unfortunately, in reality WiFi transmitter and receiver are not time-synchronized, hence there exists a time-varying random phase offset in each CSI sample. This random phase offset prevents us from directly using the CSI phase information for respiration sensing. In addition, there is only one WiFi antenna available in smartphone, we are not able to cancel out the phase offset using the CSI ratio which requires two antennas. We therefore use amplitude only for respiration sensing. According to Eq. 16, the amplitude of CSI can be calculated:

$$Amp^2 = H_s^2 + A^2 \frac{sin(\frac{1}{2}dL\frac{u(t)}{\lambda}2\pi)}{sin(\frac{1}{2}d\frac{u(t)}{\lambda}2\pi)}^2 + AH_s \frac{sin(\frac{1}{2}dL\frac{u(t)}{\lambda}2\pi)}{sin(\frac{1}{2}d\frac{u(t)}{\lambda}2\pi)} cos((k_0+\frac{1}{2}dL)\frac{u(t)}{\lambda}2\pi - \theta_0) \tag{17}$$

where θ_0 is the phase of static path $H_s(f,t)$. As described in Section 4.1., the value of $k_i = k_0 + d(i-1)$ is ranged from 0 to 2, implying that the phase change of each trigonometric function in Eq. 17 is no more than $2\pi\frac{u(t)}{\lambda}$.

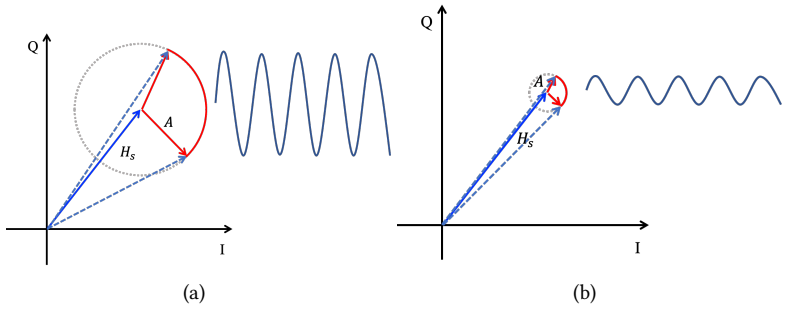

Fig. 7. Quality of CSI amplitude is influenced by the energy of the static path and the dynamic path. (a) Static energy and dynamic energy keep balanced (b) Static energy is much larger than dynamic energy

Study [24] shows that chest displacement $u(t)$ caused by respiration is ranged from 0.5 mm to 12.6 mm, far more less than the wavelength of 5.24 GHz (i.e., 5.7 cm). Thus, the peaks/valleys of all trigonometric function in Eq. 17 are all related to breathing in and out.

For trigonometric functions, the period will not change if we add, subtract, multiply or divide two trigonometric functions with the same period. Basically, we can think that is peaks/valleys observed in Eq. 17 are all caused by chest displacement during respiration. Base on this, we now simplify Eq. 17 as follows.

$$Amp_t^2 = H_s^2 + (A^2 + AH_s)sin(k \cdot \frac{2\pi}{\lambda} \cdot u(t) - \theta_0) \tag{18}$$

where the range of k is between 0 and 1. When chest displacement goes up and down during respiration, the value of each trigonometric function increases or decreases correspondingly. We can hence relate the peak/valley of each trigonometric function to $u(t)$. In a nutshell, the ambient reflection signal model informs that *the received CSI waveforms would contain the respiration induced signal with the same frequency.*

From Eq. 18, we observe that the volatility of CSI amplitude is directly affected by the value of $A^2 + AH_s$. As we mentioned before, H_s is the energy of the static path and A represents the energy of the dynamic path. To ensure the quality of received signals, the value of H_s and A should increase or decrease at the same time. If A is much smaller than H_s, the waveform caused by respiration is easily buried into high static energy. As shown in Fig. 7., the respiration pattern is much clearer when the static energy and dynamic energy are balanced.

Study [13] shows that more than 70% of energy is transferred via the LoS (i.e., the static path). Our model uses ambient reflection signals, and in this case the dynamic path energy is much weaker than the static path energy. As a result, ambient reflected signals can be easily buried into strong static energy.

Based on the analysis above, it is easy to obtain the following two properties of our ambient reflection signal model for respiration sensing.

- P1: CSI amplitudes from ambient reflected signals change with chest displacement caused by respiration.
- P2: Respiration-induced CSI patterns can be easily buried into noise when the power of dynamic path is significantly smaller than static path due to the block of dynamic path.

4.3 Model Verification

We now verify the properties of our ambient reflection signal model through experiments.

Experiment for P1: As shown in Fig. 8 (a), we conduct an experiment in a real home with household furniture and decoration. We use a WiFi router ASUS RT-AC86U and an off-the-shelf smartphone Nexus 5 as the transceiver

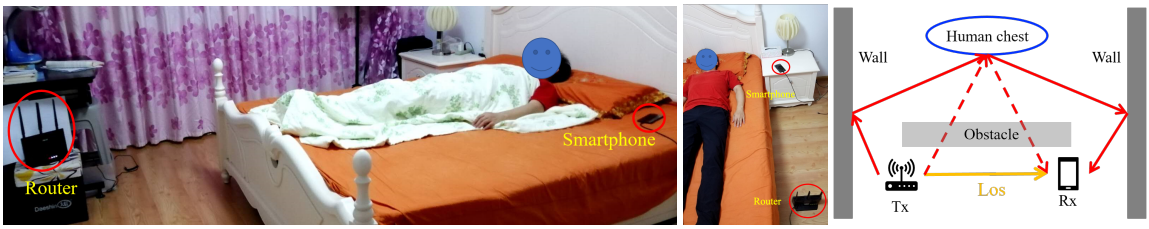

(a) (b) (c)

Fig. 8. Experimental setting for P1(a) and P2 (b), (c) illustrates the experimental setup of P2

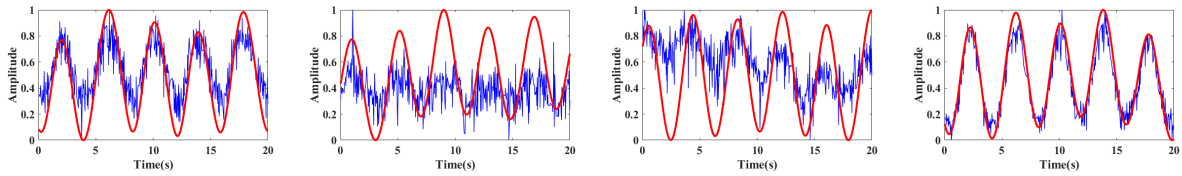

(a) (b) (c) (d)

Fig. 9. Denoised CSI amplitudes from (a) NLoS, (b) LoS-visible, (c) LoS-blocked by glass, and (d) LoS-blocked by metal plate

pair. The central frequency of the router is set as 5.745 GHz. The router is located at a corner of the room under the table and the smartphone is placed beside the pillow. A subject lies in bed and breathes in 15 bpm, the ground truth is obtained by a commercial device. In this experiment, the LoS between the transceiver pair is blocked by human body. Fig. 9 (a) shows CSI amplitudes selected from random sub-carriers after preprossessing, where the ground truth is illustrated in red line and raw CSI obtained is illustrated in blue line. We observe that the result matches the ground truth well.

Experiment for P2: In this experiment, we change the setup and let the LoS stay clear of blocking, as shown in Fig.8 (b) and (c). We observe a strong static power along the direct path from transmitter to receiver.

We now conduct experiments to evaluate the impact of the static power by blocking the LoS using different obstacles, e.g., glass and metal. WiFi signals passing through different mediums may have different power diminution. As we know, the diminution by a metal plate is more than glass. Fig. 9. shows the denoised CSI amplitudes from (b) LoS, (c) blocked by glass, and (d) blocked by metal plate, where the ground truth obtained from wearable sensor is marked in red line and raw CSI is marked in blue line. While we cannot observe a clear respiration pattern in Fig. 9 (b), Fig. 9 (d) shows a clear respiration pattern when the LoS is blocked by the metal plate. We observe a weaker and noisy respiration pattern in Fig. 9 (c) since the signal penetrability through glass is stronger than metal.

This suggests that when we deploy router and smartphone in a real environment, we should avoid the scenario shown in Fig. 8 (b) where the LoS is visible while it's preferable to have the LoS blocked and only ambient reflected signal can be used for sensing. We have to say the LoS scenario is one limitation of our current work.

5 EVALUATION

We conduct comprehensive experiments to evaluate the performance of WiPhone. We first describe the system set-up for data collection, and then present the evaluation results from a series of experiments.

5.1 Data Collection

We use an ASUS RT-AC86U WiFi router as transmitter, and three smartphones (Google's Nexus 5, Google's Nexus 6, and Google's Nexus 6P) as transceiver. From our experiments using different smartphones, we observe consistent raw CSI signals and sensing range. We hence, for simplicity, use a Google's Nexus 5 smartphone as receiver in most of the experiments. The router operates at a central frequency of 5.745 GHz with a bandwidth of 80 MHz and broadcasts 50 packets per second. We collect CSI data from the smartphone using Nexmon [29], and process the data with MATLAB at a DELL Precision 5520 laptop (Intel Xeon E3-1505M v6 CPU and 8 GB RAM). Note that using Nexmon, we are able to obtain about 52 sub-carriers for respiration sensing.

We recruit 8 volunteers (i.e., 3 males and 5 females), aged from 14 to 71 years old. Data collection is done in a real residential apartment with an area of 126 m^2 which consists of two bedrooms, one living room, one study room and one bathroom. All the subjects are told to breath normally. The ground truth of their respiration rates is ranged from 14 bpm to 22 bpm. We collect a total of 113 hours of data for our experiments. The ground truth of respiration rates is collected using a commercial device (i.e., Neulog Respiration Monitor Belt logger sensor NUL-236 [16])

5.2 Scenario 1: In the Same Room

In this experiment, we focus on the first scenario where WiFi router and smartphone are placed in the same room, i.e., bedroom. The room size is 4.74 m × 3.33 m, the bed measures 2 m by 1.8 m with a height of 0.45 m, the smartphone is 4.3 m away from the router as the crow flies. The experimental setup follows the scenario presented in Fig. 8 (a). where the router is placed at the corner of the room with its antennas pointing vertically and the smartphone is placed near the pillow on the bed. The subject lies in bed, covered with a quilt, and may have different postures, i.e., supine, prone, left and right, during experiments.

	Person1	Person2	Person3	Person4	Person5	Person6	Person7	Person8
spine	0.17	0.15	0.21	0.23	0.25	0.20	0.18	0.25
pone	0.21	0.26	0.33	0.37	0.36	0.28	0.31	0.37
left	0.20	0.32	0.23	0.32	0.32	0.27	0.27	0.32
right	0.20	0.24	0.22	0.36	0.36	0.22	0.27	0.32

Fig. 10. Confusion matrix for mean error

Fig. 10 shows the confusion matrix for mean error. The result reveals that the maximum mean error is 0.4 bpm. It implies that WiPhone achieves full detection rate (i.e., defined when the detection error is less than 0.5 bpm [45]). Among all the postures, the supine posture has the minimum mean error than other postures. No significant variation is found in the mean error among different subjects.

5.3 Scenario 2: In Different Rooms through a Wall

In this experiment, we focus on the second scenario where WiFi router and smartphone are located in different rooms with a wall inbetween. Fig. 11. shows the floor plan of the apartment where a red circle and green triangle represents router and smartphone, respectively. We have the following setups.

- Setup 1: The router is placed in Study room and the subject lies in bed in Bedroom 1 and the smartphone is placed beside the pillow. (Router and smartphone are labelled with "1" in Fig. 11.)
- Setup 2: The router is placed in Study room, and the subject sits on chair in front of a desk in Bedroom 1 with the smartphone alongside her/him. (Router and smartphone are labelled with "2" in Fig. 11.)
- Setup 3: The router is placed on the TV cabinet with a height of 30 cm in Living room, and the subject sits on chair in front of a desk in Study room with the smartphone alongside her/him. (Router and smartphone are labelled with "3" in Fig. 11.)
- Setup 4: The router is placed at the corner of Study room, and the subject sits on chair in front of a dining table in Living room while the smartphone is placed on the table. (Router and smartphone are labelled with "4" in Fig. 11.)

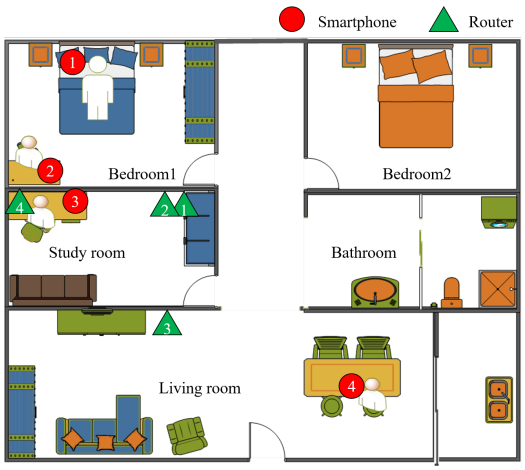

Fig. 11. Experimental settings for Scenario 2

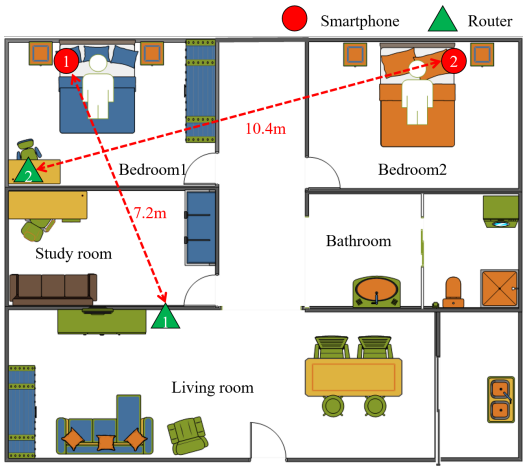

Fig. 12. Experimental settings for Scenario 3

For each setup, there exists a wall inbetween the receiver which blocks the LoS. In Setups 2, 3 and 4, the smartphone is randomly placed on the table. As shown in Fig. 13., the mean error of respiration rate for each of the setups is less than 0.5 bpm, demonstrating the respiration sensing capability of WiPhone through a wall. The result from the Setup 1 (i.e., the lying scenario) achieves the best performance of 0.22 bpm than the siting scenarios, i.e., Setup 2 (0.37 bpm), Setup 3 (0.35 bpm) and Setup 4 (0.32 bpm). This is probably because lying presents less motion as compared to sitting. Since such motions are not relevant to respiration, hence they will introduce noise by the motion of other part of human body.

5.4 Scenario 3: In Different Rooms through Walls

In this experiment, we evaluate the sensing ability of WiPhone through multiple walls, and discover the sensing range distance in a home environment. We set up experiments with a range of the direct distance between router and smartphone up to 10 meters through multiple walls inbetween. Fig. 12 illustrates two setups.

Setup 1: The router is placed on the TV cabinet in Room 1. The subject lies in bed with smartphone placed beside the pillow in Room 2. The direct distance between router and smartphone is about 7.2 m, going through two walls.

Setup 2: The router is placed at the corner of Room 2. The subject lies in bed with smartphone placed beside the pillow in Room 3. The direct distance between router and smartphone is about 10.4 m, going through two

walls and a wardrobe. Note that in reality the coverage of a commodity WiFi router in indoor environments is around 10 m [45].

Fig. 14 show the respiration pattern extracted by WiPhone, where first line represents the left respiration for Setup 1, and right for Setup 2. While the result in Setup 2 is noisy than that in Setup 1, we can still observe a clear respiration pattern from both setups.

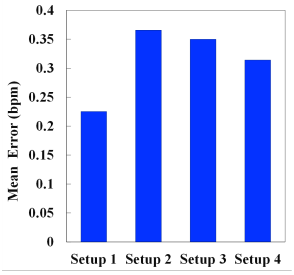

Fig. 13. Mean error of respiration rate in Scenario 2.

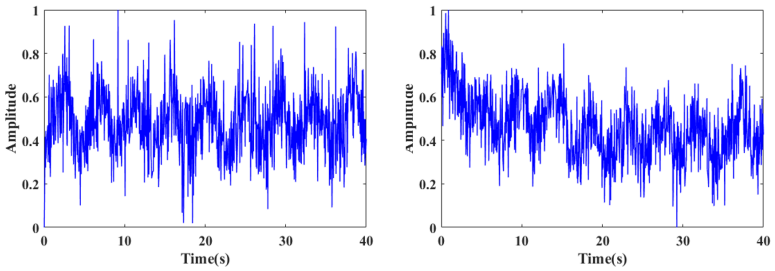

Fig. 14. Respiratory patterns obtained from Scenario 3 Setup 1 (left) and Setup 2 (right)

5.5 Performance in Abnormal Respiration

In this experiment, we evaluate WiPhone's performance under abnormal respiration. We use the same scenario, i.e., router and smartphone are placed in the same room, presented in Section 5.2. We conduct the experiment based on the symptoms of tachypnea and apnea. For tachypnea, a subject first breaths in her/his normal respiration rate and then double the respiration rate. For apnea, a subject holds her/his breath for a short while (i.e., 22 s) during normal breathing.

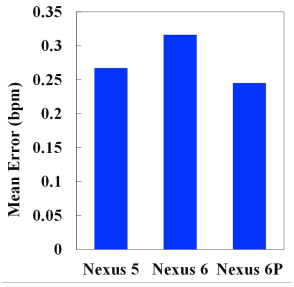

Fig. 15. Mean error of respiration rate in different type of smartphones.

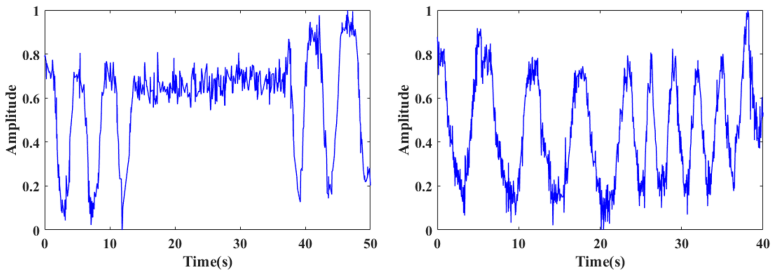

Fig. 16. Respiratory Patterns obtained from abnormal respiration

As shown in Fig. 16, in both cases, WiPhone is able to extract signal patterns precisely and detect the symptoms.

5.6 Different Smartphones

In this experiment, we evaluate the performance of WiPhone using different smartphones, i.e., Google's Nexus 5, Nexus 6 and Nexus 6P. The placement of router and smartphone is the same as the scenario of Sec. 5.2 and Fig.8(a), where the router is placed at the corner of the room and the smartphone is placed near the subject on the bed.

We first use Nexus 5 as receiver to collect CSI signals, we repeat the experiment by replacing smartphone with Nexus 6 and Nexus 6P at the same location. In all experiments, we use ASUS RT-AC86U WiFi router as transmitter and configure a central frequency of 5.745G Hz and a bandwidth of 80M Hz. As shown in Fig. 15, the mean error of respiration rate for each smartphone is less than 0.5 bpm and the difference between different smartphones is relatively small, demonstrating the effectiveness of WiPhone in different types of smartphone.

5.7 Limitations

From our experiments, we verify the effectiveness of monitoring human respiration in NLoS scenarios using ambient reflection signal. The ambient reflection model explains the relationship between ambient reflection signals and chest displacement caused by respiration. However, WiPhone may fail to work if there are other human motions, e.g., hand or body movements, just like other WiFi-based human respiration systems.

In addition, WiPhone does not work in the presence of multiple targets. It is a well-known challenge to separate the signals reflected off multiple targets and achieve multi-target sensing. One solution has been proposed in MultiSense [44] to simultaneously monitor the respiration of multiple persons by leveraging the multiple antennas widely available at commodity WiFi devices. However, such method is not applicable to smartphone that typically has only one available antenna. With more antennas built into smartphone in the near future, the solution in [44] may become feasible. We may also leverage multiple sub-carriers that analogize to multiple antennas used in MultiSense for multi-person respiration sensing.

6 CONCLUSION

Contactless respiration monitoring with WiFi CSI is promising to be deployed in real-world environments. However, existing respiration monitoring systems mainly work in LoS scenario which is not always realistic in real life since the LoS between the randomly deployed router and WiFi receivers can be easily blocked. This paper presents a smartphone based respiration monitoring system using ambient reflected signal model. We propose an ambient reflection model in the NLoS setting which well complements to the existing direct reflection model in the LoS setting. The proposed reflection signal model offers a practical solution to monitoring human respiration in real home environments. For our future work, we plan to apply our ambient reflection signal model for other challenging WiFi sensing applications such as continuous activity recognition.

ACKNOWLEDGMENTS

This research is supported by NSFC 62061146001, PKU-Baidu Funded Project 2019BD005, PKU-NTU Collaboration Project, Australian Research Council (ARC) Discovery Project grants DP180103932 and DP190101888.

REFERENCES

[1] 2004. Breathing adapted radiotherapy of breast cancer: reduction of cardiac and pulmonary doses using voluntary inspiration breath-hold. *Radiotherapy and Oncology* 72, 1 (2004), 53 – 60. https://doi.org/10.1016/j.radonc.2004.03.012

[2] Heba Abdelnasser, Khaled A Harras, and Moustafa Youssef. 2015. UbiBreathe: A Ubiquitous non-Invasive WiFi-based Breathing Estimator. (2015).

[3] Fadel Adib, Hongzi Mao, Zachary Kabelac, Dina Katabi, and Robert C. Miller. 2015. Smart Homes that Monitor Breathing and Heart Rate. (2015).

[4] Magnus Borga and Hans Knutsson. 2001. A canonical correlation approach to blind source separation. *Report LiU-IMT-EX-0062 Department of Biomedical Engineering, Linkping University* (2001).

[5] M. E. Celebi, Y. A. Aslandogan, and P. R. Bergstresser. 2005. Mining biomedical images with density-based clustering. In *International Conference on Information Technology: Coding Computing.*

[6] M Daszykowski, B Walczak, and D. L Massart. 2001. Looking for natural patterns in data : Part 1. Density-based approach. *Chemometrics Intelligent Laboratory Systems* 56, 2 (2001), 83–92.

[7] Amy Diane Droitcour et al. 2006. *Non-contact measurement of heart and respiration rates with a single-chip microwave doppler radar.* Ph.D. Dissertation. Citeseer.

[8] A. D. Droitcour, O. Boric-Lubecke, and G. T. A. Kovacs. 2009. Signal-to-Noise Ratio in Doppler Radar System for Heart and Respiratory Rate Measurements. *IEEE Transactions on Microwave Theory & Techniques* 57, 10 (2009), 2498–2507.

[9] A. D. Droitcour, O. Boric-Lubecke, V. M. Lubecke, J. Lin, and G. T. A. Kovacs. 2004. Range correlation and I/Q performance benefits in single-chip silicon Doppler radars for noncontact cardiopulmonary monitoring. *Microwave Theory Techniques IEEE Transactions on* 52, 3 (2004), 838–848.

[10] Ashish Ghosh, Anindya Halder, Megha Kothari, and Susmita Ghosh. 2008. Aggregation pheromone density based data clustering. *Information ences* 178, 13 (2008), 2816–2831.

[11] Ludger Grote. 2019. The global burden of sleep apnoea. *The Lancet Respiratory Medicine* 7, 8 (2019).

[12] Peter Hillyard, Anh Luong, Alemayehu Solomon Abrar, Neal Patwari, Krishna Sundar, Robert Farney, Jason Burch, Christina Porucznik, and Sarah Hatch Pollard. 2018. Experience: Cross-Technology Radio Respiratory Monitoring Performance Study. In *Proceedings of the 24th Annual International Conference on Mobile Computing and Networking (MobiCom '18)*. Association for Computing Machinery, New York, NY, USA, 487–496. https://doi.org/10.1145/3241539.3241560

[13] Hristo Hristov. 2000. *Fresnel Zones in Wireless Links, Zone Plate Lenses and Antennas*.

[14] Igor Immoreev and Teh-Ho Tao. 2008. UWB radar for patient monitoring. *IEEE Aerospace and Electronic Systems Magazine* 23, 11 (2008), 11–18.

[15] Hua Jiang, Jing Li, Shenghe Yi, Xiangyang Wang, and Xin Hu. 2011. A new hybrid method based on partitioning-based DBSCAN and ant clustering. *Expert Systems with Applications* 38, 8 (2011), 9373–9381.

[16] Wern Kam, Waleed Soliman Mohammed, Gabriel Leen, Mary O'Keeffe, Kieran O'Sullivan, Sinead O'Keeffe, and Elfed Lewis. 2017. Compact and low-cost optical fiber respiratory monitoring sensor based on intensity interrogation. *Journal of Lightwave Technology* 35, 20 (2017), 4567–4573.

[17] Joshua Chong Yue Lai, Ying Xu, Erry Gunawan, Eric Chern-Pin Chua, Arash Maskooki, Yong Liang Guan, Kay-Soon Low, Cheong Boon Soh, and Chueh-Loo Poh. 2011. Wireless sensing of human respiratory parameters by low-power ultrawideband impulse radio radar. *IEEE Transactions on Instrumentation and Measurement* 60, 3 (2011), 928–938.

[18] Antonio Lazaro, David Girbau, and Ramon Villarino. 2010. Analysis of vital signs monitoring using an IR-UWB radar. *Progress In Electromagnetics Research* 100 (2010), 265–284.

[19] Changzhi Li, Victor M Lubecke, Olga Boric-Lubecke, and Jenshan Lin. 2013. A review on recent advances in Doppler radar sensors for noncontact healthcare monitoring. *IEEE Transactions on microwave theory and techniques* 61, 5 (2013), 2046–2060.

[20] Jian Liu, Yan Wang, Yingying Chen, Jie Yang, Xu Chen, and Jerry Cheng. 2015. Tracking vital signs during sleep leveraging off-the-shelf wifi. In *Proceedings of the 16th ACM International Symposium on Mobile Ad Hoc Networking and Computing*. 267–276.

[21] Xuefeng Liu, Jiannong Cao, Shaojie Tang, and Jiaqi Wen. 2014. Wi-Sleep: Contactless sleep monitoring via WiFi signals. In *2014 IEEE Real-Time Systems Symposium*. IEEE, 346–355.

[22] Xuefeng Liu, Jiannong Cao, Shaojie Tang, Jiaqi Wen, and Peng Guo. 2015. Contactless respiration monitoring via off-the-shelf WiFi devices. *IEEE Transactions on Mobile Computing* 15, 10 (2015), 2466–2479.

[23] Xuefeng Liu, Jiannong Cao, Shaojie Tang, Jiaqi Wen, and Peng Guo. 2016. Contactless Respiration Monitoring Via Off-the-Shelf WiFi Devices. *IEEE Transactions on Mobile Computing* 15, 10 (2016), 2466–2479.

[24] C. Lowanichkiattikul, M. Dhanachai, C. Sitathanee, S. Khachonkham, and P. Khaothong. 2016. Impact of chest wall motion caused by respiration in adjuvant radiotherapy for postoperative breast cancer patients. *SpringerPlus* (2016).

[25] L. Robert Mogue and Boerje Rantala. 1988. Capnometers. *Journal of Clinical Monitoring* 4, 2 (1988), 115–121.

[26] Rajalakshmi Nandakumar, Shyamnath Gollakota, and Nathaniel Watson. 2015. Contactless Sleep Apnea Detection on Smartphones. In *the 13th Annual International Conference*.

[27] R. Paradiso. 2003. Wearable health care system for vital signs monitoring. In *4th International IEEE EMBS Special Topic Conference on Information Technology Applications in Biomedicine, 2003.* 283–286.

[28] Claudia Plant, Stefan J. Teipel, Annahita Oswald, Christian B?Hm, Thomas Meindl, Janaina Mourao-Miranda, Arun W. Bokde, Harald Hampel, and Michael Ewers. 2010. Automated detection of brain atrophy patterns based on MRI for the prediction of Alzheimer's disease. *Neuroimage* 50, 1 (2010), 162–174.

[29] Matthias Schulz, Jakob Link, Francesco Gringoli, and Matthias Hollick. 2018. Shadow Wi-Fi: Teaching Smartphones to Transmit Raw Signals and to Extract Channel State Information to Implement Practical Covert Channels over Wi-Fi. In *Proceedings of the 16th Annual International Conference on Mobile Systems, Applications, and Services (MobiSys '18)*. Association for Computing Machinery, New York, NY, USA, 256–268. https://doi.org/10.1145/3210240.3210333

[30] Matthias Schulz, Daniel Wegemer, and Matthias Hollick. 2017. Nexmon: The C-based Firmware Patching Framework. https://nexmon.org

[31] N. H. Shariati and E. Zahedi. 2005. Comparison of selected parametric models for analysis of the photoplethysmographic signal. In *2005 1st International Conference on Computers, Communications, Signal Processing with Special Track on Biomedical Engineering*. 169–172.

[32] Andrew G Stove. 1992. Linear FMCW radar techniques. In *IEE Proceedings F (Radar and Signal Processing)*, Vol. 139. IET, 343–350.

[33] James D Taylor. 2018. *Ultra-wideband radar technology*. CRC press.

[34] S. Venkatesh, C. R. Anderson, N. V. Rivera, and R. M. Buehrer. 2006. Implementation and analysis of respiration-rate estimation using impulse-based UWB. In *Military Communications Conference*.
[35] Hao Wang, Daqing Zhang, Junyi Ma, Yasha Wang, Yuxiang Wang, Dan Wu, Tao Gu, and Bing Xie. 2016. Human respiration detection with commodity wifi devices: do user location and body orientation matter?. In *Proceedings of the 2016 ACM International Joint Conference on Pervasive and Ubiquitous Computing*. 25–36.
[36] Wei Wang, Alex X Liu, Muhammad Shahzad, Kang Ling, and Sanglu Lu. 2015. Understanding and modeling of wifi signal based human activity recognition. In *Proceedings of the 21st annual international conference on mobile computing and networking*. 65–76.
[37] Xuyu Wang, Chao Yang, and Shiwen Mao. 2017. PhaseBeat: Exploiting CSI phase data for vital sign monitoring with commodity WiFi devices. In *2017 IEEE 37th International Conference on Distributed Computing Systems (ICDCS)*. IEEE, 1230–1239.
[38] Xuyu Wang, Chao Yang, and Shiwen Mao. 2017. TensorBeat: Tensor decomposition for monitoring multiperson breathing beats with commodity WiFi. *ACM Transactions on Intelligent Systems and Technology (TIST)* 9, 1 (2017), 1–27.
[39] K. WATANABE. [n.d.]. Noninvasive measurement of heartbeat, respiration, snoring and body movements of a subject in bed via a pneumatic method. 52 ([n. d.]).
[40] Dan Wu, Daqing Zhang, Chenren Xu, Hao Wang, and Xiang Li. 2017. Device-free WiFi human sensing: From pattern-based to model-based approaches. *IEEE Communications Magazine* 55, 10 (2017), 91–97.
[41] Dan Wu, Daqing Zhang, Chenren Xu, Yasha Wang, and Hao Wang. 2016. WiDir: walking direction estimation using wireless signals. In *Proceedings of the 2016 ACM international joint conference on pervasive and ubiquitous computing*. 351–362.
[42] Shichao Yue, Hao He, Hao Wang, Hariharan Rahul, and Dina Katabi. 2018. Extracting multi-person respiration from entangled rf signals. *Proceedings of the ACM on Interactive, Mobile, Wearable and Ubiquitous Technologies* 2, 2 (2018), 86.
[43] Youwei Zeng, Dan Wu, Ruiyang Gao, Tao Gu, and Daqing Zhang. 2018. FullBreathe: Full Human Respiration Detection Exploiting Complementarity of CSI Phase and Amplitude of WiFi Signals. *Proceedings of the ACM on Interactive, Mobile, Wearable and Ubiquitous Technologies* 2, 3 (2018), 148.
[44] Youwei Zeng, Dan Wu, Jie Xiong, Jinyi Liu, Zhaopeng Liu, and Daqing Zhang. 2020. MultiSense: Enabling multi-person respiration sensing with commodity wifi. *Proceedings of the ACM on Interactive, Mobile, Wearable and Ubiquitous Technologies* 4, 3 (2020), 1–29.
[45] Youwei Zeng, Dan Wu, Jie Xiong, Enze Yi, Ruiyang Gao, and Daqing Zhang. 2019. Farsense: Pushing the range limit of wifi-based respiration sensing with csi ratio of two antennas. *Proceedings of the ACM on Interactive, Mobile, Wearable and Ubiquitous Technologies* 3, 3 (2019), 1–26.
[46] Youwei Zeng, Dan Wu, Jie Xiong, and Daqing Zhang. 2020. Boosting WiFi Sensing Performance via CSI Ratio. *IEEE Pervasive Computing* (2020).
[47] Daqing Zhang, Hao Wang, and Dan Wu. 2017. Toward centimeter-scale human activity sensing with Wi-Fi signals. *Computer* 50, 1 (2017), 48–57.
[48] Fusang Zhang, Daqing Zhang, Jie Xiong, Hao Wang, Kai Niu, Beihong Jin, and Yuxiang Wang. 2018. From Fresnel Diffraction Model to Fine-Grained Human Respiration Sensing with Commodity Wi-Fi Devices. *Proceedings of the ACM on Interactive, Mobile, Wearable and Ubiquitous Technologies* 2, 1 (2018), 1–23.
[49] Liming Zhou, Philip K. Hopke, and Prasanna Venkatachari. 2006. Cluster analysis of single particle mass spectra measured at Flushing, NY. *Analytica Chimica Acta* 555, 1 (2006), 47–56.

APPENDIX

We now extend the above scenario with two ambient-reflected points to other scenarios–more than two points or less than two points. Again, our analysis will be focused on the left side of the human chest). Fig. 17(a) illustrates the scenario where there is no reflection point on the left side, and we have:

$$\Delta d_A(t) = length(A - R_t - u(t)) - length(A - R_t - u_0) \tag{19}$$

Fig. 17(b) illustrates the scenario where there are two ambient-reflected points on the left side. We can see that $\triangle AR_1R_{1t}$ and $\triangle A^{'}R_1R_{1t}$,$\triangle$, $A^{'}R_2R_{2t}$ and $\triangle A^{''}R_2R_{2t}$ are two pairs of congruent equilateral triangles, and we have:

$$\Delta d_A(t) = length(A^{''} - u_0) - length(A^{''} - u_(t)) \tag{20}$$

The scenario shown in Fig. 17(b) can be extended to more than two ambient-reflected points, and the same analysis will be applied. Obviously, $d_A(t)$ has a maximum range of $u(t)$ no matter how many ambient-reflected points inbetween.

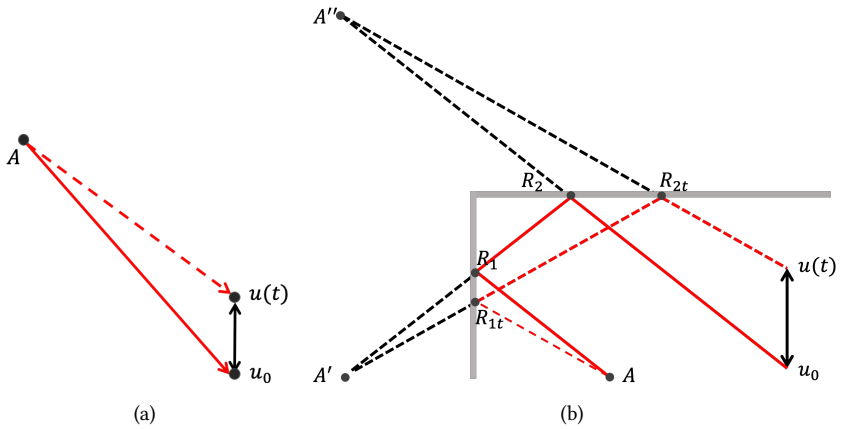

Fig. 17. Ambient reflection model with (a) no reflection point and (b) two reflection points on one side

While the right side follows the same principle. We hence generalize our model for multiple ambient-reflected points as follows.

$$d_i(t) = d_{i0} + k_i u(t) \ (0 < k_i < 2) \tag{21}$$

The value range of K_i implies that the ambient-reflected path length change caused by respiration should be less than twice of chest displacement.